Mutifuntional GdPO4:Eu3+ Hollow Spheres: Synthesis and Magnetic and Luminescent Properties

ARTICLE *in* INORGANIC CHEMISTRY · NOVEMBER 2011

Impact Factor: 4.76 · DOI: 10.1021/ic200867a · Source: PubMed

6 AUTHORS, INCLUDING:

Hongpeng You
Chinese Academy of Sciences
178 PUBLICATIONS **3,414** CITATIONS
SEE PROFILE

Yanhua Song
Jilin University
88 PUBLICATIONS **1,842** CITATIONS
SEE PROFILE

Inorganic Chemistry

ARTICLE

pubs.acs.org/IC

Mutifuntional $GdPO_4$:Eu^{3+} Hollow Spheres: Synthesis and Magnetic and Luminescent Properties

Lihui Zhang, Meili Yin, Hongpeng You,* Mei Yang, Yanhua Song, and Yeju Huang

State Key Laboratory of Rare Earth Resource Utilization, Changchun Institute of Applied Chemistry, Chinese Academy of Sciences, Changchun, 130022 and Graduate University of the Chinese Academy of Sciences, Beijing 100049, P. R. China

Supporting Information

ABSTRACT: Mondispersed submicrometer $GdPO_4$:Eu^{3+} hollow spheres were synthesized via an effective one-pot hydrothermal process. These hollow spheres have the average diameter of 200 nm, and the shell thickness is about 20 nm. The surface of the spheres consists of a number of nanorods with diameters of about 10 nm and lengths of about 50−80 nm. Both magnetic and luminescent properties of the obtained Eu^{3+}-doped $GdPO_4$ hollow spheres were investigated. The hysteresis plot ($M-H$) analysis result indicates their paramagnetic property. The fluorescence spectra demonstrate that they emit orange-red color light originated from the $^5D_0 \rightarrow {}^7F_J$ transitions of the Eu^{3+} ions. Therefore, the obtained $GdPO_4$ hollow spheres hold promise for encapsulate drugs with controlled release. Moreover, the $GdPO_4$:Eu^{3+} hollow spheres are attributes for bimodal magnetic resonance imaging (MRI)/optical bioimaging labeling.

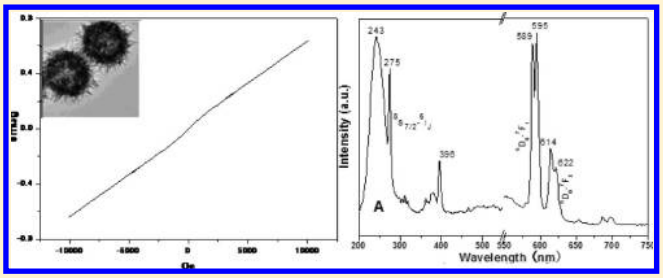

1. INTRODUCTION

Because of a large number of unpaired electrons (as many as seven), the Gd^{3+} ion is strongly paramagnetic, and complex species of Gd^{3+} ion have been commonly used as a magnetic resonance imaging (MRI) contrast agent. There are MRI contrast agents for positive-intensity images such as gadolinium(III) chelates Gadolinium-DiethyleneTriaminePentaacetic Acid (Gd-DTPA),[1,2] Gd_2O_3,[3−5] and $Gd_2O(CO_3)_2 \cdot H_2O$.[5] For these Gd-based materials, the development of multifunctional particulate agents for bimodal MRI/optical bioimaging detection is required. Particularly, nanoparticles combining fluorescence and magnetic resonance imaging have received much attention because they ally the high sensitivity of the fluorescence phenomenon to the high spatial resolution of MRI. In the literature, for example, bifunctional probes consisting of Gd_2O_3 nanoparticles conjugated with different fluorescent dyes (fluorescein isothiocyanate (FITC), Rhodamine B isothiocyanate (RBITC) , or Cyanine 5-N-hydroxysuccinimidyl Ester (Cy5-NHS) ester)[6] and Tb^{3+}-Doped Gd_2O_3 nanocrystals[3] were directly demonstrated in fluorescent labeling and MRI contrast agent properties. However, to our best knowledge, there have been no reports of the magnetic behaviors of $GdPO_4$ species yet. Meanwhile, as an alternative to dye molecules and QDs, rare-earth lanthanide phosphate fluorescent labels, especially Eu- and Tb-phosphate nanoparticles, maintain comparatively higher quantum yields (up to 61%), lower photobleaching potential, expected low toxicity, and high chemical stability, all of which are promising attributes for biological labeling applications.[7−9] In recent years, lanthanide phosphate nanoparticles have been used as inorganic fluorescent labels in cell biology research. These fluorescent nanoparticles can internalize in cells and do not appear to detrimentally affect cell viability or induce toxicity after internalization. Moreover, they retain their intrinsic fluorescent properties, which can be in turn clearly visualized by confocal fluorescence microscopy. Therefore, by combining the magnetic property of the nanoparticle matrix ($GdPO_4$) and the fluorescent property of the doping ions (Eu^{3+}), multifunctional nanoparticles can be tailored.

Materials with hollow and porous nanostructures have a potentially low density and have a large specific area and surface permeability that are sensitive and favorable for biological applications. Additionally, hollow spheres are widely used as controlled-release capsules for drugs, dyes, cosmetics, artificial cells, and catalysts. Paramagnetic hollow and porous nanostructures are promising for encapsulate drugs for controlled release during magnetic delivery. Superparamagnetic hollow and paramagnetic porous Gd_2O_3 particles of about 200 nm were obtained by biological gelatin particles as center cores acting as shape and structure directors.[4] Herein, $GdPO_4$:Eu^{3+} hollow spheres with the average diameter of 200 nm were prepared. Both magnetic and luminescent properties of the obtained Eu^{3+}-doped $GdPO_4$ hollow spheres were investigated in detail. These properties, along with the drug release behaviors (see the Supporting Information), make it possible to use $GdPO_4$:Eu^{3+} hollow spheres as a multifunctional material.

2. EXPERIMENTAL SECTION

2.1. Materials. $Ln(NO_3)_3$ (Ln = Gd, Eu) (1 M) stock solutions were prepared by dissolving the corresponding metal oxide in concentrated

Received: April 25, 2011
Published: October 04, 2011

dx.doi.org/10.1021/ic200867a | *Inorg. Chem.* 2011, 50, 10608–10613

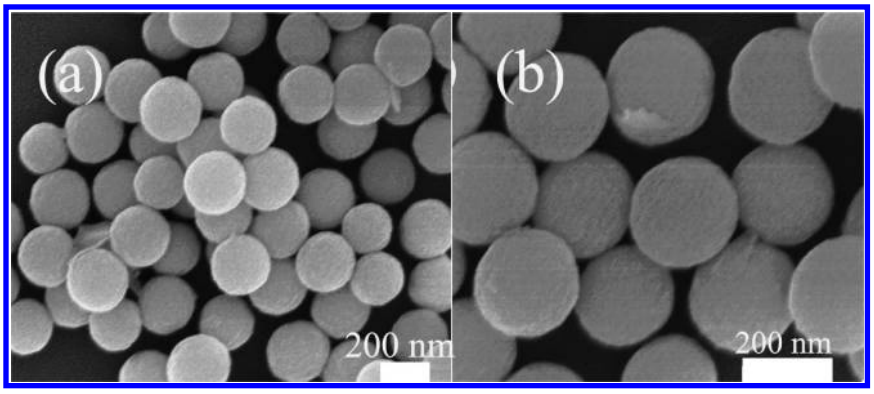

Figure 1. (a) Low- and (b) high-magnification SEM image of $Gd(OH)CO_3$ colloidal spheres after the homogeneous precipitation process.

HNO_3 at elevated temperature. Gd_2O_3 (99.99%) and Eu_2O_3(99.99%) were purchased from Beijing Chemical Co. All chemicals were analytical grade reagents and used directly without further purification.

2.2. Preparation of $GdPO_4$ Hollow Spheres. *Synthesis of $Gd(OH)CO_3$ Colloid Spheres.* $Gd(OH)CO_3$ colloid spheres were prepared by a urea-based homogeneous precipitation process as follows: 1 mL of $Gd(NO_3)_3$(1M) and 3 g of urea $[CO(NH_2)_2]$ were dissolved in deionized water,[10] and the total volume of the solution was about 50 mL. The resultant solution was then reacted at 85 °C for 2 h in the oil bath.

Synthesis of $GdPO_4$ Hollow Spheres. $GdPO_4$ hollow spheres were prepared after the following hydrothermal process:[11] in a typical synthesis, the as-obtained 1 mmol of $Gd(OH)CO_3$ precipitation was redispersed into deionized water by ultrasonic treatment for half an hour. $NH_4H_2PO_4$ (0.115 g) dissolved in proper deionized water was dripped into the dispersion. A total of 0.1 g of cetyltrimethylammonium bromide (CTAB) was added to the above suspensions. The reaction solution was given the hydrothermal treatment at 200 °C for 12 h to get $GdPO_4$ hollow spheres. A similar process was employed to prepare $GdPO_4$:5% Eu^{3+} hollow spheres using a stoichiometric amount of $Eu(NO_3)_3$ aqueous solutions instead of $Gd(NO_3)_3$ solution for the precursors at the initial stage as described above.The obtained white products of $GdPO_4$ and $GdPO_4$:Eu^{3+} hollow spheres were carefully collected after washing with deionized water and alcohol and dried at 60 °C for 24 h in air.

2.3. Characterization. The samples were characterized by powder X-ray diffraction (XRD) performed on a diffractometer (Bruker). The morphology and composition of the sample was inspected using a field emission scanning electron microscope (SEM; S-4800, Hitachi). Transmission electron microscopy (TEM) images were obtained using a TECNAI G2 transmission electron microscope operating at 200 kV. Hysteresis loops were collected on a Quantum Design superconducting quantum interference device (SQUID) magnetometer (LakeShore 7307) at 300 K. The excitation and emission spectra were recorded with a Hitachi F-4500 spectrophotometer equipped with a 150 W xenon lamp as the excitation source at room temperature.

3. RESULTS AND DISCUSSION

3.1. $GdPO_4$ Hollow Sphere and the Formation Mechanism. Figure 1 gives the SEM image of $Gd(OH)CO_3$ colloidal spheres after the homogeneous precipitation process. One can find that the obtained $Gd(OH)CO_3$ sample exhibits uniform monodisperse colloid spheres with smooth surfaces and has an average diameter of about 200−220 nm. The as-prepared $Gd(OH)CO_3$ colloidal spheres acted as the precursor of the following reaction.

Figure 2c shows the XRD pattern of the as-prepared product that the $Gd(OH)CO_3$ colloidal spheres were treated with $NH_4H_2PO_4$ at 200 °C for 12 h in the hydrothermal process.

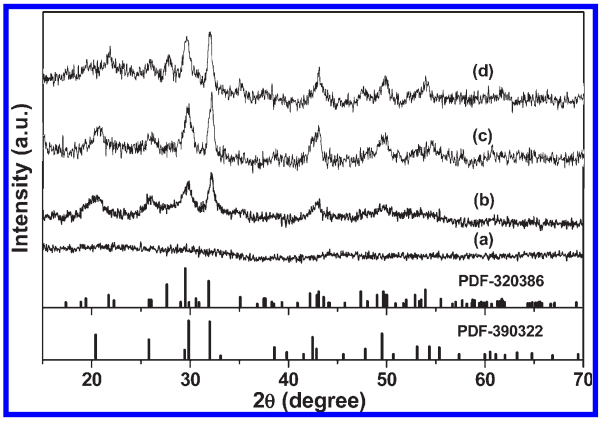

Figure 2. XRD patterns of the obtained $GdPO_4$ samples after the hydrothermal process (a: 30 min; b: 2 h; c: 12 h) and the calcined sample after 750 °C for 2 h (d).

All diffraction peaks can be indexed as pure hexagonal phase for $GdPO_4 \cdot nH_2O$ (JCPDS no. 39-0232). In the hexagonal structure of $GdPO_4 \cdot nH_2O$, the Gd^{3+} is coordinated to eight oxygen atoms in a manner as to leave open, oxygenlined channels along the hexagonal axis with a diameter of approximately 0.6 nm, and the water contributes to the stabilization of the hexagonal structure since it gets incorporated into the open spaces which form tunnels along the crystalline axis in the hexagonal structure.[12,13] When the product was annealed at 750 °C for 2 h, the crystal water molecule is removed from the hexagonal phase and it is transformed into the monoclinic phase (Figure 2d). The diffraction peaks are found to be consistent with the monoclinic $GdPO_4$ (JCPDS no. 32-0386). The results reveal the formation of pure $GdPO_4$ phase after the hydrothermal process. Otherwise, the remaining amorphous $Gd(OH)CO_3$ precursor could be thermally decomposed into Gd_2O_3 under annealing and form the diffraction peaks under XRD excitation.

In order to investigate the existence of the hydration and phase transition of the obtained products, TG-DTA measurements were performed (Figure 3). TGA data of as-prepared $GdPO_4$ powder showed a weight loss (11.4 wt %) between room temperature and 800 °C. The first 3.3 wt % loss was observed below 120 °C followed by a further 7.8 wt % between 240 and 630 °C. These two courses have already been observed and interpreted as the evaporation of moisture present on the material's surface (the first of the processes), followed by the release of zeolitically bound water (at the higher temperature).[14−16] Therefore,

the second weight losses can be assigned to the dehydration of the hexagonal form of lanthanum orthophosphate, which indicates that the obtained phosphate hydrate should be $GdPO_4 \cdot H_2O$. According to the revised literature,[17−20] different temperature values in the range of 375 to 900 °C are given for the rhabdophane-type $LaPO_4 \cdot nH_2O$ (hexagonal) to monazite-type

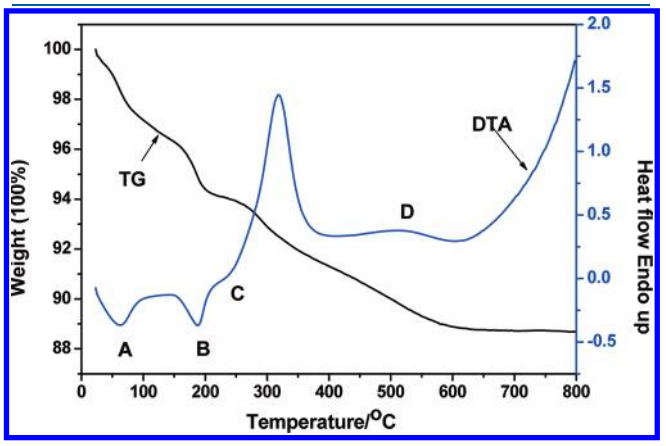

Figure 3. TG-DTA curves of the as-prepared $GdPO_4$ sample after the hydrothermal process.

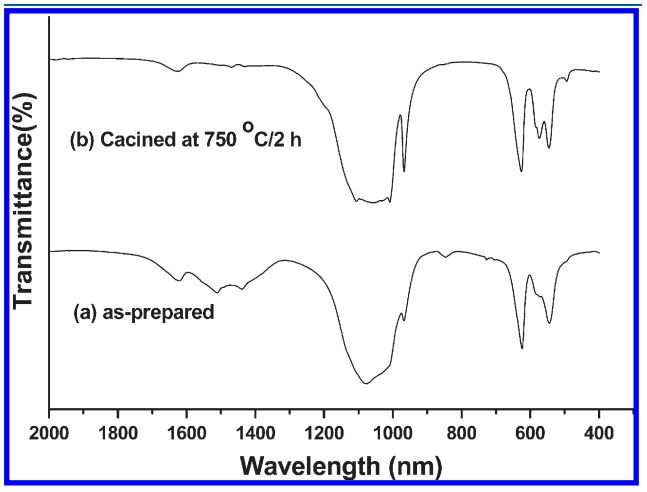

Figure 4. FT−IR spectra of the as-prepared $GdPO_4$ sample (a) and the sample annealed at 750 °C (b).

$LaPO_4$ (monoclinic) phase transition. In this study, the exothermic peak at 517 °C can be assigned to this transformation for $GdPO_4$.

Moreover, FT−IR spectra of both the as-prepared $GdPO_4$ sample and the sample annealed at 750 °C were performed to confirm the phase transition (Figure 4). FT−IR measurements of the as-prepared sample indicated that the absorption bands, in the range of 475−1200 cm^{-1}, were attributable to the active vibrations of tetrahedral PO_4^{3-}. The bands centered at 525 and 625 cm^{-1} are attributed to the O−P−O bending vibrations, and the band centered at 1075 cm^{-1} is ascribed to the asymmetry stretching vibration of the PO_4^{3-} groups. The spectra include strong bands at about 1630 cm^{-1}, characteristic of the deformation vibrations of water molecules. The presence of the bands in the spectra is justified by the incorporation of zeolitic water molecules into the hexagonal structure. The above analysis indicates the formation of hexagonal $GdPO_4 \cdot H_2O$ phase. The bands centered at 1438 and 1511 cm^{-1} are attributed to the COO− vibrations from $Gd(OH)CO_3$, which indicate that there is still little amount of $Gd(OH)CO_3$ remaining in the final product. The FT−IR spectrum of the $GdPO_4$ samples heat-treated at 750 °C shows the splitting of the bands in the range of 1007−1107 cm^{-1} and 540−580 cm^{-1} and in increased absorption at about 967 cm^{-1}. That is due to the formation of monazite in poorer symmetry, which is reflected in splitting in the FT−IR spectrum.

Figure 5 shows the SEM and TEM images of the $GdPO_4$ hollow spheres after the hydrothermal treatment of 12 h. As shown from the low-magnification SEM image, the monodisperse spherical morphology is well-preserved after the hydrothermal process, and the spherical particles have a diameter distribution ranging from 220 to 240 nm. However, their surfaces became somewhat roughened because of the formed aggregates of numerous nanorods. To investigate the real composition of the as-synthesized product, energy-dispersive X-ray (EDX) spectrum analysis was carried out and the result is shown in Figure 6. It confirms the presence of elements Gd, P, and O in the product and the obtained atomic ratio of Gd:P is 1:1.1, which is approaching the theoretical value in $GdPO_4$. Transmission electron microscopy (TEM) was carried out to verify the hollow structure of the microspheres. The strong contrast between the dark edges and the pale center further confirms that all the spherical particles have a large hollow structure. The large hollow cavity is about 180−200 nm in size, and the shell thickness is 20 nm. The surface of the spheres consists of a number of nanorods with diameters of

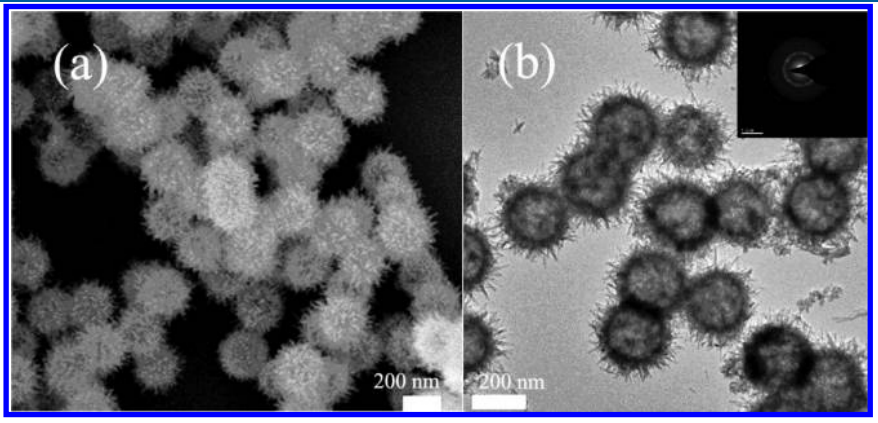

Figure 5. SEM image (a), TEM image (b) and the corresponding SAED pattern (inset) of the $GdPO_4$ hollow spheres after the hydrothermal treatment of 12 h.

dx.doi.org/10.1021/ic200867a |*Inorg. Chem.* 2011, 50, 10608–10613

about 10 nm and lengths of about 50−80 nm. The selected area electron diffraction (SAED) pattern (inset in Figure 5b) shows the diffraction ring pattern, confirming the polycrystalline nature of $GdPO_4$ hierarchical hollow spheres.

To elucidate the formation mechanism, the time-dependent experiments were carried out at 200 °C for 30 min and 2 h, respectively. The products were collected at the different reaction times. As shown from the TEM image of 30 min, some tiny nanorods are generated on the surface (Figure 7a). A careful observation reveals that a very thin layer of $GdPO_4 \cdot H_2O$ has already formed closely on the surface of $Gd(OH)CO_3$ spheres. However, no obvious XRD peaks appear in the XRD pattern-(Figure 2a), indicating a little $GdPO_4$ has formed in the early stage of 30 min. When it prolonged to 2 h, a large void between the core and shell could be observed, and the core becomes very little, which indicates that the reaction process is very fast (Figure 7b). The core and shell is connected by filament-like bridges, which might act as fast transport paths for the delivery of the remaining core to the shell, resulting in the ultimate hollow structure.[21] Correspondingly, the $GdPO_4 \cdot H_2O$ phase was obtained in the XRD pattern of 2 h (Figure 2b).

On the basis of the above experiment results, a possible schematic illustration of the overall formation process of $GdPO_4$ hollow spheres is presented in Figure 7d, and the main chemical reactions can be written as follows:

$$Gd(OH)CO_3 \rightarrow Gd^{3+} + OH^- + CO_3^{2-} \quad (1)$$

$$Gd^{3+} + PO_4^{3-} \rightarrow GdPO_4 \quad (2)$$

$Gd(OH)CO_3$ colloid spheres ionized slowly to produce Gd^{3+}, OH^-, and CO_3^{2-} ions in solution (eq 1), and they were located around the surface of the $Gd(OH)CO_3$ spheres. When PO_4^{3-} ions were introduced to the solution, the reaction (eq 2) at the solid−liquid interface leads to quick formation of a layer of $GdPO_4$ shell, which were aggregates of $GdPO_4$ rods around the external surface of the $Gd(OH)CO_3$ spheres. The outer $GdPO_4$ shell prevents a direct chemical reaction, and further reaction relies on diffusion of Gd^{3+} and PO_4^{3-} through the shell. Due to the different ionic radii between Gd^{3+} and PO_4^{3-}, a net directional flow of Gd^{3+} ions is through the $Gd(OH)CO_3$ shell, which is balanced by an opposite flow of vacancies. Thus, an interior void is obtained on the basis of a unbalanced interdiffusion process through the reaction interface.[21] As the reaction proceeds in time, more Gd^{3+} ions diffuse out to the shell, leading to the decrease of the $Gd(OH)CO_3$ core and the mergence of the initial voids in the inner. This results in the formation of bridges of material between the core and the shell. These bridges provide a fast transport path for outward diffusion of Gd^{3+} ions. The process could persist until the core disappears. This evolution process could provide evidence that the Kirkendall effect is responsible for the formation of $GdPO_4$ hollow spheres.

Since $Gd(OH)CO_3$ colloidal spheres act as the precursor, the size of $GdPO_4$ hollow spheres can be easily tuned by that of $Gd(OH)CO_3$. $GdPO_4$ hollow spheres in the range of 80−110 nm can be obtained by utilizing $Gd(OH)CO_3$ colloidal spheres in diameters of 70−100 nm (see Figure S1 in Supporting Information). Moreover, temperature affected the formation of $GdPO_4$ hollow spheres, especially when the size of $Gd(OH)CO_3$ colloidal spheres was about 100 nm. If we set the reaction temperature at 200 °C, several fractures of hollow spheres would exist in the product. That might be attributed to the small size and the high reaction rate. When the temperature is 150 °C, entire $GdPO_4$ hollow spheres of about 100 nm in size could be

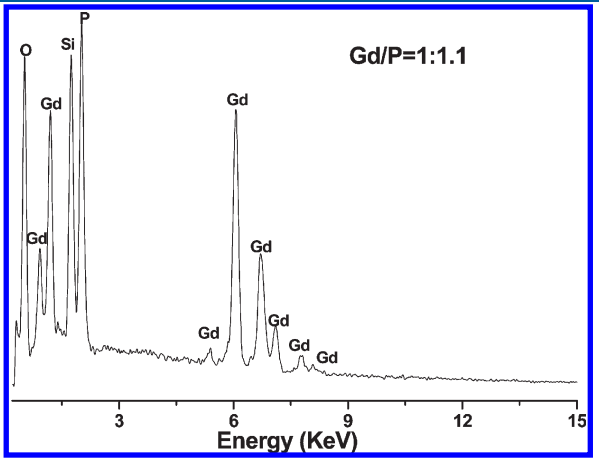

Figure 6. EDX spectrum of the $GdPO_4$ hollow spheres.

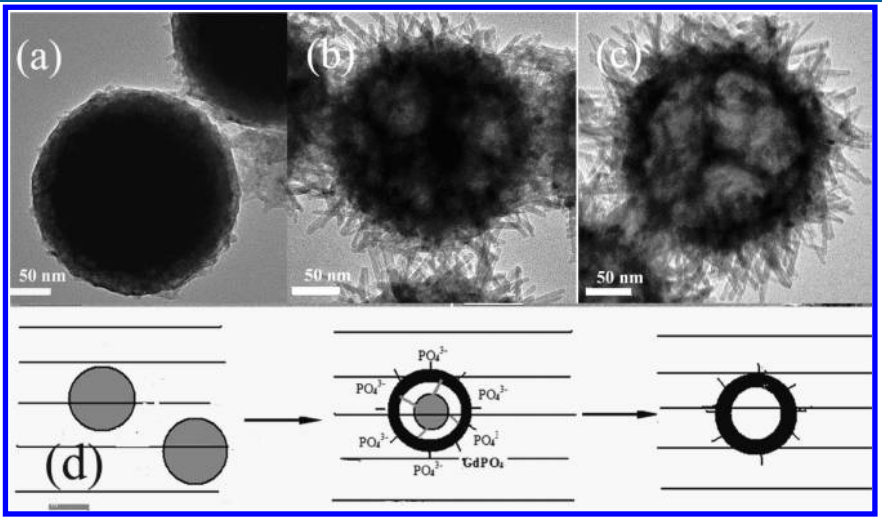

Figure 7. (a−c): TEM images of the as-prepared $GdPO_4$ sample (a: 30 min; b: 2 h; c: 12 h); (d) schematic illustration of the formation process of $GdPO_4$ hollow submicrometer-sized spheres based on the Kirkendall effect.

dx.doi.org/10.1021/ic200867a |*Inorg. Chem.* 2011, 50, 10608–10613

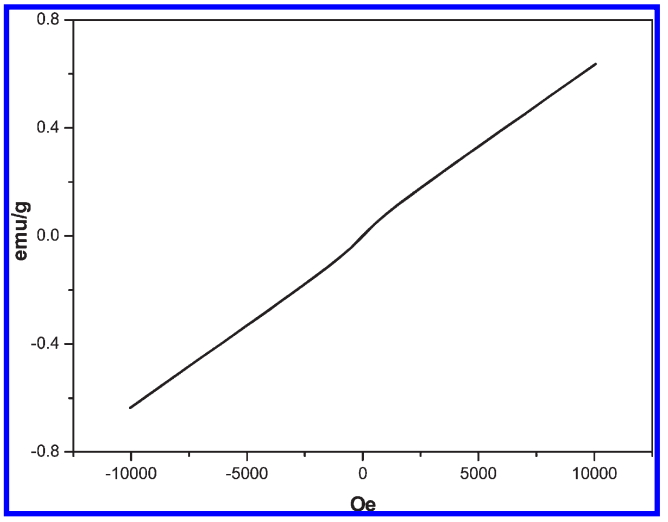

Figure 8. Magnetization plots of $GdPO_4:Eu^{3+}$ hollow spheres as a function of the applied fields (−10 and +10 kOe) at 300 K.

obtained. Moreover, $GdPO_4$ hollow spheres have a small size, which has many advantages over larger ones when they penetrate the cell membrane.

3.2. Magnetism. Figure 8 shows SQUID magnetometry magnetization-magnetic field (*M-H*) plots at 300 K. As the strength of the applied magnetic field increased, the ideal linear correlation between the magnetization and the applied magnetic field in the $GdPO_4:Eu^{3+}$ was obtained, indicating that $GdPO_4$ possesses paramagnetism. The mass magnetic susceptibility value of the as-prepared $GdPO_4$ is determined to be 6.4×10^{-5} emu/g·Oe. The magnetization at 10 kOe is around 0.64 emu/g. The paramagnetic property of the Gd^{3+} ions come from seven unpaired inner 4f electrons, which are closely bound to the nucleus and effectively shielded by the outer closed shell electrons $5s^25p^6$ from the crystal field. The magnetic moments associated with the Gd^{3+} ions are all localized and noninteracting, giving rise to paramagnetism. The $GdPO_4:Eu^{3+}$ hollow spheres with paramagnetic property might be applied as MRI contrast agent.

3.3. Photoluminescence. The photoluminescence (PL) excitation and emission spectra for the hexagonal $GdPO_4:Eu^{3+}$ hollow spheres and the monoclinic sample obtained after heat treatment are shown in Figure 9. For the hexagonal $GdPO_4:Eu^{3+}$ sample, the excitation spectrum consists of a strong broadband centered at 243 nm and several narrow bands. The strong band is attributed to the charge transfer band (CTB) between the O^{2-} and Eu^{3+} ions. The narrow bands are due to the f−f transitions within the Eu^{3+} $4f^6$ electron configuration. The observation of the $Gd^{3+8}S_{7/2} \rightarrow {}^6I_J$ transition located at 275 nm in Eu^{3+} excitation spectra indicates that an energy transfer from Gd^{3+} multiplets ^6I_J (at 4.49 eV) to electronic levels of Eu^{3+} occurs. In this case, the density of states above $^5L_6$ (at 3.16 eV) is so high that there is rather a continuum of levels in the relevant energy range. The maximum absorption line at around 396 nm is assigned to the $^7F_0 \rightarrow {}^5L_6$ transition of the Eu^{3+} ions. However, a small shift of the CTB could be observed for the monoclinic $GdPO_4:Eu^{3+}$, with the maximum appearing at 246 nm (Figure 7b). Previous studies of the CTB of Eu^{3+} in different host lattices have indicated that its position depends both on the Eu−O bond length and on the coordination environment about Eu^{3+}.[22] The variation is proportional to the Eu−O distance: the longer the

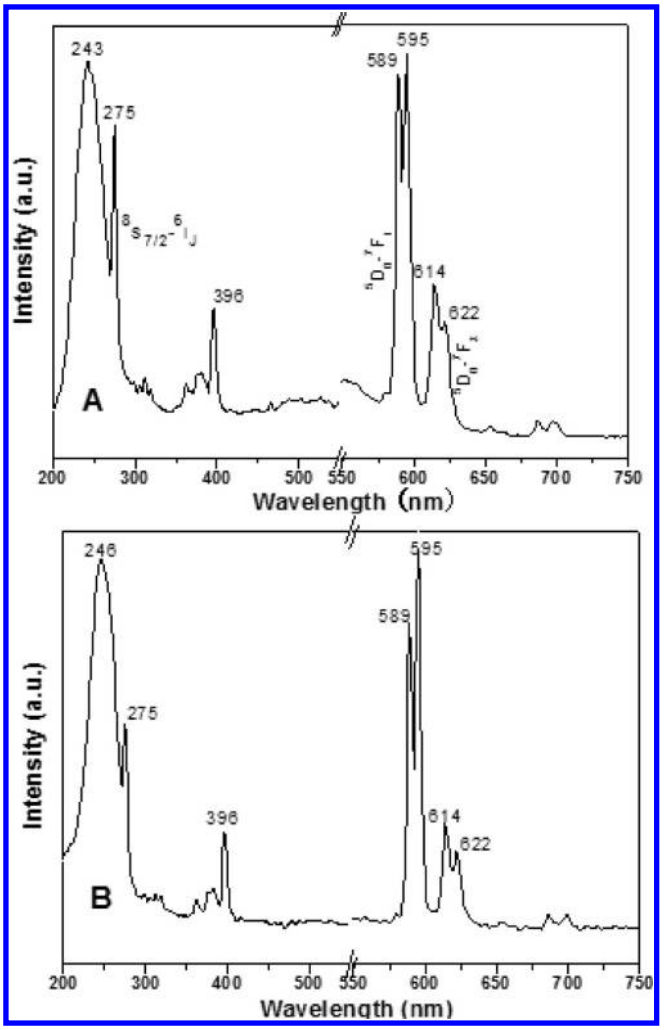

Figure 9. PL excitation and emission spectra for the as-prepared hexagonal $GdPO_4:Eu^{3+}$ sample (A) and the monoclinic sample obtained after heat treatment (B).

Eu−O bond, the longer is the wavelength of the CTB. Hence, the small red shift observed for monoclinic $GdPO_4:Eu^{3+}$ indicates that the average Eu−O bond distance is somewhat longer in monoclinic $GdPO_4:Eu^{3+}$ sample than in their hexagonal ones. For the hexagonal $GdPO_4:Eu^{3+}$ sample, the emission spectrum of as-prepared hexagonal $GdPO_4:Eu^{3+}$ hollow spheres is composed of sharp lines ranging from 570 to 720 nm, which are attributed to the transitions from the excited $^5D_0$ level to ^7F_J ($J = 0, 1, 2, 3, 4$) levels of the Eu^{3+} ions, respectively. It exhibits orange-red color due to the main emission transitions $^5D_0 \rightarrow {}^7F_1$ line in 590 nm and $^5D_0 \rightarrow {}^7F_1$ line in 614 nm, respectively, and the $^5D_0 \rightarrow {}^7F_1$transition exhibits the most intense emission. As we know, when Eu^{3+} ions occupy inversion center sites, the $^5D_0 \rightarrow {}^7F_1$ transition is relatively strong, while the $^5D_0 \rightarrow {}^7F_1$ transition is relatively weak. The results indicate that Eu^{3+} ions occupy inversion center sites in $GdPO_4:Eu^{3+}$ hollow spheres. From the emission spectrum of monoclinic $GdPO_4:Eu^{3+}$ sample (Figure 7b), it could be revealed that the change of the phase structure has a little effect on the location of their luminescent lines. However, the spectral splitting of monoclinic-type $GdPO_4:Eu^{3+}$ is some different from hexagonal ones, owing to the stark effect of different crystal fields.

dx.doi.org/10.1021/ic200867a |*Inorg. Chem.* 2011, 50, 10608–10613

4. CONCLUSION

In summary, monodispersed $GdPO_4$ hollow spheres of submicrometer scale were successfully obtained by a facile one-pot hydrothermal process via the colloidal spheres of $Gd(OH)CO_3$ as the starting core materials reacted with $NH_4H_2PO_4$ solution based on the Kirkendall effect. The hysteresis plot ($M-H$) analysis result indicates their paramagnetic property. The investigation of the luminescent property reveals that the $GdPO_4$:Eu^{3+} hollow spheres emit the typical orange-red color light originated from the $^5D_0 \rightarrow {}^7F_J$ transitions of the Eu^{3+} ions. These results indicate that the obtained hollow spheres may have potential applications in cell biology, diagnosis, and drug release. Moreover, our strategy developed herein is also expected to be used for the fabrication of other phosphate materials with hollow structures in the future.

■ ASSOCIATED CONTENT

Supporting Information. Figures of sizes of precursors and the hollow spheres and in vitro cumulative release of metformin from the loaded-$GdPO_4$ hollow spheres; additional experimental section and results and discussion. This material is available free of charge via the Internet at http://pubs.acs.org.

■ AUTHOR INFORMATION

Corresponding Author
*E-mail: hpyou@ciac.jl.cn.

■ ACKNOWLEDGMENT

This work is financially supported by the National Natural Science Foundation of China (Grant No. 20771098), the NSFC Fund for Creative Research Groups (Grant No. 20921002), and the National Basic Research Program of China (973 Program, Grant No. 2007CB935502).

■ REFERENCES

(1) Caravan, P. *Chem. Soc. Rev.* **2006**, *35*, 512.
(2) Raymond, K. N.; Pierre, V. C. *Bioconjugate Chem.* **2005**, *16*, 3.
(3) Petoral, R. M.; Soderlind, F.; Klasson, A.; Suska, A.; Fortin, M. A.; Abrikossova, N.; Selegard, L.; Kall, P. O.; Engstrom, M.; Uvdal, K. *J. Phys. Chem. C* **2009**, *113*, 6913.
(4) Huang, C. C.; Liu, T. Y.; Su, C. H.; Lo, Y. W.; Chen, J. H.; Yeh, C. S. *Chem. Mater.* **2008**, *20*, 3840.
(5) Li, B. F.; Su, C. H; Lo, Y. W.; Lin, W. T.; Chen, J. H.; Yeh, C. S. *Adv. Funct. Mater.* **2008**, *18*, 766.
(6) Bridot, J. L.; Faure, A. C.; Laurent, S.; Rivière, C.; Billotey, C.; Hiba, B.; Janier, M.; Josserand, V.; Coll, J. L.; Elst, L. V.; Muller, R.; Roux, S.; Perriat, P.; Tillement, O. *J. Am. Chem. Soc.* **2007**, *129*, 5076.
(7) Patra, C. R.; Bhattacharya, R.; Patra, S.; Basu, S.; Mukherjee, P.; Mukhopadhyay, D. *J. Nanobiotechnol.* **2006**, *4*, 11.
(8) Patra, C. R.; Bhattacharya, R.; Patra, S.; Basu, S.; Mukherjee, P.; Mukhopadhyay. *Clin. Chem.* **2007**, *53*, 2029.
(9) Zhang, F.; Wong, S. S. *ACS Nano* **2010**, *4*, 99.
(10) Jia, G.; You, H. P.; Liu, K.; Zheng, Y. H.; Zhang, H. J. *Langmuir* **2010**, *26*, 5122.
(11) Zhang, L. H.; Jia, G.; You, H. P.; Liu, K.; Yang, M.; Song, Y. H.; Zheng, Y. H.; Huang, Y. J.; Guo, N.; Zhang, H. J. *Inorg. Chem.* **2010**, *49*, 3305.
(12) Mooney, R. C. L. *J. Chem. Phys.* **1948**, *16*, 1003.
(13) Mooney, R. C. L. *Acta Crystallogr.* **1950**, *3*, 337.
(14) Matraszek, A.; Radominska, E.; Szczygiel, I. *J. Therm. Anal. Calorim.* **2011**, *103*, 813.
(15) Kijkowska, R. *Thermochim. Acta* **2003**, *404*, 81.
(16) Chen, P.; Mah, T. *J. Mater. Sci.* **1997**, *32*, 3863.
(17) Lucas, S.; Champion, E.; Bregiroux, D.; Bernache-Assollant, D.; Audubert, F. *J. Solid State Chem.* **2004**, *177*, 1302–1312.
(18) Fujishiro, Y.; Ito, H.; Sato, T.; Okuwaki, A. *J. Alloys Compd.* **1997**, *252*, 103.
(19) Rajesh, K.; Sivakumar, B.; Krishna Pillai, B.; Mukundan, P.; Warrier, K. G. K.; Nair, V. R. *Mater. Lett.* **2004**, *58*, 1687.
(20) Gallini, S.; Jurado, J. R.; Colomer, M. T. *Chem. Mater.* **2005**, *17*, 4154.
(21) Yin, Y. D.; Rioux, R. M.; Erdonmez, C. K.; Hughes, S.; Somorjai, G. A.; Alivisatos, A. P. *Science* **2004**, *304*, 711.
(22) Zhang, W. W.; Zhang, W. P.; Xie, P. B.; Yin, M.; Chen, H. T.; Jing, L.; Zhang, Y. S.; Lou, L. R.; Xia, S. D. *J. Colloid Interface Sci.* **2003**, *262*, 588.